AD-A267 713

Fiber Strength Utilization in Carbon/Carbon Composites

Prepared by

R. J. ZALDIVAR and G. S. RELLICK
Mechanics and Materials Technology Center
The Aerospace Corporation

and

J. M. YANG
Department of Materials Science and Engineering
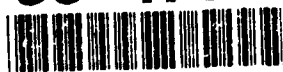University of California, Los Angeles

15 May 1993

DTIC

S **ELECTE**
AUG 0 4 1993
B **D**

Prepared for

SPACE AND MISSILE SYSTEMS CENTER
AIR FORCE MATERIEL COMMAND
Los Angeles Air Force Base
P. O. Box 92960
Los Angeles, CA 90009-2960

93-17309 425
002

Engineering and Technology Group

THE AEROSPACE CORPORATION
El Segundo, California

93 8 3 036

Norton Compton, Lt. Col. USAF
Project Officer

W. Kyle Sneddon, Capt. USAF
MOIE Program Manager

REPORT DOCUMENTATION PAGE

1a. REPORT SECURITY CLASSIFICATION	1b. RESTRICTIVE MARKINGS
Unclassified	

2a. SECURITY CLASSIFICATION AUTHORITY	3. DISTRIBUTION/AVAILABILITY OF REPORT
	Approved for public release; distribution unlimited
2b. DECLASSIFICATION/DOWNGRADING SCHEDULE	

4. PERFORMING ORGANIZATION REPORT NUMBER(S)	5. MONITORING ORGANIZATION REPORT NUMBER(S)
TR-92(2935)-1	SMC-TR-93-33

6a. NAME OF PERFORMING ORGANIZATION	6b. OFFICE SYMBOL (If applicable)	7a. NAME OF MONITORING ORGANIZATION
The Aerospace Corporation Technology Operations		Space and Missile Systems Center

6c. ADDRESS (City, State, and ZIP Code)	7b. ADDRESS (City, State, and ZIP Code)
El Segundo, CA 90245-4691	Los Angeles Air Force Base Los Angeles, CA 90009-2960

8a. NAME OF FUNDING/SPONSORING ORGANIZATION	8b. OFFICE SYMBOL (If applicable)	9. PROCUREMENT INSTRUMENT IDENTIFICATION NUMBER
		F04701-88-C-0089

8c. ADDRESS (City, State, and ZIP Code)	10. SOURCE OF FUNDING NUMBERS			
	PROGRAM ELEMENT NO.	PROJECT NO.	TASK NO.	WORK UNIT ACCESSION NO.

11. TITLE (Include Security Classification)

Fiber Strength Utilization in Carbon/Carbon Composites

12. PERSONAL AUTHOR(S)

Zaldivar, R J.; Rellick, Gerry S.; and Yang, J M.

13a. TYPE OF REPORT	13b. TIME COVERED FROM _____ TO _____	14. DATE OF REPORT (Year, Month, Day) 15 May 1993	15. PAGE COUNT 31

16. SUPPLEMENTARY NOTATION

17. COSATI CODES			18. SUBJECT TERMS (Continue on reverse if necessary and identify by block number)
FIELD	GROUP	SUB-GROUP	Carbon/Carbon Composites, Carbon Fibers, Polyarylacetylene

19. ABSTRACT (Continue on reverse if necessary and identify by block number)

The utilization of tensile strength of carbon fibers in unidirectional carbon/carbon (C/C) composites was studied for a series of four mesophase-pitch-based carbon fibers in a carbon matrix derived from a polyarylacetylene (PAA) resin. The fibers had moduli of 35, 75, and 130 Mpsi. Composite processing conditions ranged from the cured-resin state to various heat-treatment temperatures (HTTs) from 1100 to 1750°C for the C/Cs. Room-temperature tensile strength and modulus were measured for the various processing conditions, and were correlated with SEM observations of fracture surfaces, fiber and matrix microstructures, and fiber/matrix interphase structures. Fiber tensile strength utilization (FSU) is defined as the ratio of apparent fiber strength in the C/C to the fiber strength in an epoxy-resin-matrix composite. Carbonization heat treatment to 1100°C results in a brittle carbon matrix that bonds strongly with the three lower modulus fibers, resulting in matrix-dominated failure at FSU values of 24 to 35%. However, the composite with the 130-Mpsi modulus filament had an FSU of 79%. It is attributed to a combination of tough

20. DISTRIBUTION/AVAILABILITY OF ABSTRACT	21. ABSTRACT SECURITY CLASSIFICATION
[X] UNCLASSIFIED/UNLIMITED ☐ SAME AS RPT. ☐ DTIC USERS	Unclassified

22a. NAME OF RESPONSIBLE INDIVIDUAL	22b. TELEPHONE (Include Area Code)	22c. OFFICE SYMBOL

DD FORM 1473, 84 MAR   83 APR edition may be used until exhausted. All other editions are obsolete.

fracture within the filament itself and a weaker fiber/matrix interface. Both factors lead to crack deflection and blunting rather than to crack propagation. The presence of a weakened interface is inferred from observations of fiber pullout. Much of the FSU of the three lower modulus fibers is recovered by HTT to 2100 or 2400°C, principally as a result of interface weakening, which works to prevent matrix-dominated fracture. With HTT to 2750°C, there is a drop in FSU for all the composites; it is apparently the result of a combination of fiber degradation and reduced matrix stress-transfer capability.

PREFACE

DTIC QUALITY INSPECTED 3

Accession For	
NTIS CRA&I	☑
DTIC TAB	☐
Unannounced	☐
Justification	
By	
Distribution/	
Availability Codes	
Dist	Avail and/or Special
A-1	

1

CONTENTS

FIGURES

TABLES

I. INTRODUCTION

Over the past 20 years, the tensile strengths of both pitch-derived and PAN-derived carbon fibers have increased progressively. However, the strength utilization of such fibers in carbon/carbon (C/C) composites is still disappointingly low, of the order of only 20 to 50% of the rule-of-mixtures prediction[1] compared with carbon-fiber-reinforced epoxy composites, which typically utilize 90 to 95% of the fiber strength. Poor utilization of the reinforcement strength in C/C composites, as discussed by Jortner,[2] Leong, Zimmer, and Weitz,[3] and Fitzer and Hüttner,[4] is clearly related to the unique processing that is involved in C/C composite fabrication. Processing-related factors that may contribute to these low strength utilizations are (1) chemical attack of the fiber by matrix pyrolysis gases; (2) matrix cracking, which causes stress concentrations; (3) residual stresses in the fibers (created by thermal expansion mismatches between fiber and matrix during processing); (4) thermal-stress-induced fiber/matrix debonding, resulting in reduced fiber/matrix stress-transfer capability; (5) matrix-initiated failure of the composite caused by strongly bonded low strain-to-failure carbon matrices; and (6) high-temperature processing, which can lead to structural modifications and strength degradation in the fiber.

The objective of the current study is to expand our understanding of some of these factors. Specifically, we attempt to relate fiber tensile strength utilization to various fiber and matrix microstructural features in single-tow unidirectional composites fabricated from a polyarylacetylene (PAA)-resin-based matrix and a series of four mesophase-pitch-based fibers.

II. EXPERIMENTAL

A. Fabrication and characterization of test specimens

The fibers used in this study were mesophase-pitch-derived carbon fibers supplied by DuPont and designated E35, E75, E105, and E130, corresponding to reported moduli of 35, 75, 105, and 130 Mpsi (241, 516, 724, and 894 GPa), respectively. A compilation of manufacturer's test data is given in Table I. Each fiber tow contained 3000 filaments. The resin used in the fabrication of all the C/C composites was PAA. PAA is an experimental thermosetting resin synthesized from diethynylbenzene. It has been discussed more fully in other publications.[5-7] Unidirectional composite samples were prepared by wrapping the carbon fiber tows around an aluminum rack and impregnating them with a methyl ethyl ketone (MEK):PAA solution while maintaining the tows in slight tension. The impregnated tows were air-dried and then cured at 250 °C on the rack. Subsequent heat treatments (HTs) were performed at 1100, 2150, 2400, and 2750 °C. The tensile strength and modulus were measured using an Instron universal testing machine with a crosshead speed of 0.05 in./min (1.27 mm/min). The tabs were gripped with compression-type steel grips. A 200-lb load cell was used for all composite testing. Sample gauge length was 2 in. The procedure followed for determining the system compliance is given in ASTM D4018-81. The tabbed test specimens were vertically centered between the grip jaws, aligning them with the test machine centerline. The upper jaw was then tightened. Once visual alignment was completed, the stationary lower grip jaws were closed. Twenty samples of each fiber designation were tested for each heat-treatment temperature (HTT).

In order to set a baseline for composite strengths, we also heat-treated the bare fiber tows to the same HTTs. Following heat treatment, specimens were prepared for tensile testing following closely the procedure described in ASTM D4018-81, modified to

accommodate 2-in. gauge samples epoxy-bonded to cardboard grips. In addition, the tows were epoxy-impregnated by the same solution-drip technique used with the PAA-impregnated tows. The gauge length of all the samples was 2 in. (5.08 cm). Total specimen length was 5 in.

A major advantage of working with single-tow composites is that the total cross-sectional area of the filaments can be calculated relatively accurately. The most reliable technique is to calculate the ratio of tow lineal density (g/cm) to fiber real density (g/cm^3). This calculation can then be supported by direct measurements of filament diameter from scanning electron microscopy (SEM) and by manufacturer-supplied data.

Fiber volume fractions were calculated for selected samples from the composite cross-sectional areas obtained from photographs and from a knowledge of the total fiber area of the 3000-filament tows.

SEM was used to study fiber and matrix microstructure. Composite specimens were prepared for SEM by mounting in epoxy resin and polishing to an optical finish. The polished samples were xenon-ion-etched to enhance the distinction between glassy and graphitic-type carbon microstructures. Fracture surfaces were also examined by SEM.

As-received and heat-treated carbon fibers were examined by x-ray diffraction using copper (Kα) radiation in conjunction with a computer-controlled vertical powder diffractometer equipped with a graphite crystal monochromator and a scintillation detector. Scans were conducted at a speed of 2.4° 2θ/min and operating conditions of 45 kV and 38 mA.

III. RESULTS AND DISCUSSION

Table II shows the (002) d-spacings of the four fibers as a function of HTT. The d-spacings range initially from 0.347 nm for the E35 fiber to 0.338 nm for the E130 fiber.

7

Following HT to 2150 °C, the d-spacings for the E35 and E75 fibers decrease to 0.339 nm. After the 2400 °C HT, all the fibers have the same d-spacing of 0.338 nm; after further HT to 2750 °C, all four fibers have a d-spacing of ~0.337 nm.

For the composites, our goal ideally is to be able to calculate the actual *fiber* strength and moduli, but this is impossible to do exactly in the present study. However, it turns out that we can estimate these values reasonably accurately by applying a simple linear-elastic rule-of-mixtures model with suitable assumptions. The expression for composite modulus is

$$E_c = E_f V_f + E_m V_m \; , \tag{1}$$

where E is Young's modulus, V is volume fraction, and the subscripts c, f, and m denote composite, fiber, and matrix, respectively, and $V_m + V_f = 1$.

Obviously, if $E_m V_m \ll E_f V_f$, then $E_c \simeq E_f V_f$. This is equivalent to stating that essentially all the tensile load P is carried by the fiber; i.e., $P_c \cong P_f$, in which case, we can express the fiber strength S_f as the ratio of the composite breaking load to the fiber area A_f; i.e., $S_f \simeq P_c^u / A_f$. This approach was used to determine the strengths of both as-received and heat-treated fibers from tensile test data on epoxy-impregnated samples, and to estimate apparent fiber strength and modulus from data on the cured-PAA-resin and C/C composites.

We can test this assumption for the cured-resin-matrix composite, for which we estimate $E_m \simeq 7$ GPa; fiber volume fractions were typically ~0.25. Therefore, for the lowest modulus E35 fiber, we calculate that about 92% of the load is carried by the fibers ($E_f V_f = 0.92 \, E_c$). However, it is difficult to estimate *a priori* the carbon-matrix modulus

E_m, which depends essentially on the same factors as does fiber modulus: orientation, HTT, extent of graphitization, and microstructure. However, by plotting *apparent* fiber modulus $E_f^{app} \equiv E_c/V_f$ for the different processing conditions, from cured-resin composite to the C/Cs at various HTTs (Fig. 1), we see that the apparent fiber moduli agree well with the manufacturer-reported moduli (Table I), *and* are effectively constant from the cured-resin state through the 2150 °C HTT. This supports our assumption that the matrix contribution to the modulus is negligible for these processing conditions.

With HT to 2400 °C, the E105 and E130 apparent fiber moduli increase only slightly, whereas those for the lower modulus E35 and E75 composites increase markedly. SEM observations, presented later, reveal matrix sheath formation for all the composites at the 2400 °C HTT. This sheath structure very likely contributes to the modulus; nevertheless, it seems reasonable to attribute the large modulus increase for the E35 and E75 composites to *predominantly* the effects of fiber heat treatment rather than to a *significant* contribution from the matrix. This is suggested by the relatively narrow range of apparent fiber moduli following the 2400 °C HT, which is consistent with a tendency for the moduli of a family of fibers from the same precursor to converge with increasing HTT. It is also supported by previous work[6] with PAN-based T50 fiber unidirectionals, in which no modulus enhancement was found after the same 2400 °C HTT. In order for the modulus enhancement to be the result of a matrix sheath structure around the filament, sheath formation would be required to vary with fiber type—i.e., there would be a much larger sheath contribution in the E35 composites. While we cannot rule out this possibility conclusively, we do not believe it to be likely.

With HTT to 2750 °C, all the composites exhibit large increases in apparent fiber moduli (Fig. 1) to values exceeding 1 TPa (150 Mpsi), which is the theoretical limit of graphite basal-plane modulus. This means that the composite modulus now *must* have significant contributions from the matrix, and our simple rule-of-mixtures assumption, $E_c \equiv E_f V_f$, is no longer valid. Nevertheless, we can make reasonable estimates of the load carried by the fibers, recognizing that the modulus of the E130 fiber cannot be much more than ~140 Mpsi. We then back-calculate the true composite modulus from $E_c = V_f E_f^{app}$, where E_f^{app} is the apparent fiber modulus from Fig. 1. Since the total load carried by the fibers is $E_f V_f$, the fractional load is E_f / E_f^{app}. Therefore, for the E130 composite HT to 2750 °C, we calculate that about 73% of the load is carried by the fibers. If we assume that the modulus and volume fraction of matrix in the other three composites are the same as in the E130 composite, reasonable fiber moduli of 105, 120, and 130 Mpsi are calculated for the E35, E75, and E105 composites following the 2750 °C HTT.

To study the effects of HT on the bare (i.e., unimpregnated) fibers, as-received fiber tows were heat-treated to the various temperatures, then epoxy-impregnated and tensile-tested as a baseline for C/C composites. Results are shown in Fig. 2. (Moduli were not measured.) The tensile strengths of all four types of fibers remain unchanged through the 2150°C HT. After HT to 2400 °C, all fiber tensile strengths increase, ranging from about 10% for the E35 fiber to about 20% for the E130 fiber. Following HT to 2750 °C, the two lower modulus fibers experience essentially no change, whereas the E105 and E130 fibers increase in strength by an additional 13 and 17% relative to the 2400 °C HTT values. The tendency for the two higher modulus fibers to increase in strength with HTT to 2400 and 2750 °C, while the two lower modulus fibers first increase slightly and then remain

10

constant, correlates with the experimental observation of slight warping of the two lower modulus fibers following these HTTs. It suggests that some axial restraint of the two lower modulus fibers during HT may be necessary for maximum strength development.

Note also that our strand-measured strengths for as-received fibers are approximately 15 to 20% lower than those reported by Dupont, in spite of our shorter gauge length. This may suggest a systematic error, resulting, most likely, from the handling procedures involved in strand testing. At the same time, however, we observe that the heat-treated fibers, which involve significantly more handling, generally increase, rather than decrease, in strength, suggesting that handling procedures are not introducing significant testing artifacts. This is further supported by results (unpublished) in which we obtained good agreement between our epoxy-strand strengths and those of Amoco for unsized P100 fiber.

We define the fiber strength utilization (FSU) in the C/C composite as the ratio of the apparent fiber strength in the heat-treated C/C [$S_f(C/C)_T$] to the strength of the heat-treated bare fibers embedded in the epoxy-matrix [$S_f(epoxy)_T$]:

$$ FSU = \frac{S_f(C/C)_T}{S_f(epoxy)_T} , \tag{2} $$

where the subscript T refers to the temperature of heat treatment. The baseline fiber strengths for each HTT are those reported in Fig. 2. By substitution in the right side of Eq. (2), we also obtain:

$$ FSU = \frac{E_f(C/C)_T}{E_f(epoxy)_T} \cdot \frac{\epsilon_f(C/C)_T}{\epsilon_f(epoxy)_T} , \tag{3} $$

11

where E_f is fiber modulus and ϵ_f is fiber failure strain. The fiber failure strains were not measured directly; they were calculated as the ratio of apparent fiber strength to modulus. The stress–strain curves were always linear to failure.

As stated earlier, we did not measure $E_f(\text{epoxy})_T$—i.e., the modulus of the bare fibers following heat treatment. However, as Fig. 1 shows, the apparent fiber modulus *in the C/C* was unaffected by heat treatment through 2150 °C; therefore, we expect that the moduli of the *bare* fibers heat treated to these same temperatures ($\leq$2150 °C) would be similarly unaffected. Therefore, $E_f(\text{C/C})_T/E_f(\text{epoxy})_T \simeq 1$, which means we can also estimate FSU by

$$\text{FSU} \simeq \frac{\epsilon_f(\text{C/C})_T}{\epsilon_f(\text{epoxy})_0} \qquad (\text{HTT} \leq 2150 \text{ °C}) , \qquad (4)$$

where the zero subscript refers to as-received fibers; i.e., $\epsilon_f(\text{epoxy})_T \equiv \epsilon_f(\text{epoxy})_0$ for HTT $\leq$ 2150 °C. For HT to 2400 and 2750 °C, the moduli also become functions of HTT and Eq. (4) no longer applies.

From a practical viewpoint, it would be valid, for all HTT, to calculate the FSU relative to the as-received fiber strength. In this way we would treat the processing HTT, and interactions between fiber and matrix at that HTT, as factors that affect the magnitude of delivered fiber strength relative to that available in the starting fiber.

Figures 3a and b show plots of the apparent fiber tensile strength and FSU, respectively, in the different composites as a function of HTT; Table III summarizes the FSUs and fiber failure strains for the four composites arranged by HTT. The behavior is complex, but certain trends are suggested. After the 1100 °C HTT, the E35, E75, and E105 C/C composites experience large reductions in strength and failure strain and, hence, in FSU, relative to the same fibers in the baseline epoxy-matrix composites. In contrast, the

E130 composite experiences a much smaller reduction in fiber strength capability from 100 to 79%.

These strength differences are reflected in the fracture behavior of the composites. Fracture surfaces for the 1100 °C HTT specimens are shown in Figs. 4a–d. The E35, E75, and E105 composites all exhibit planar brittle fracture, which suggests that fracture was initiated in the brittle matrix and, because of high crack-tip stresses at the well-bonded fiber/matrix interface, propagated through the specimen. In contrast, the E130 composite reveals a tougher fracture path, as seen in the more corrugated fracture face, and distinct, although modest, filament pullout (Fig. 4d).

The approximate trend of increasing fiber strength utilization with increasing fiber modulus for the 1100 °C HTT is what we would expect based on a simple model in which (1) the fiber/matrix interface bond strength of the resin-matrix composite is weaker for the higher moduli fibers due to fewer active (edge plane) sites at these fiber surfaces; (2) the fiber/matrix bond strength in the 1100 °C HTT composite is roughly proportional to this initial resin-matrix-composite bond strength; and (3) the carbon matrix is brittle with low strain to failure. Support for this argument comes from recent measurements by Edie *et al.*[8] of interlaminar shear strengths (ILSS) of composites of these same four types of fibers in an epoxy matrix. The left-hand curve in Fig. 5 is the ILSS versus fiber moduli from Ref. 8. The ILSS can be taken as a rough measure of bond strength between the fiber and resin matrix. The right-hand curve is our C/C fiber strength utilization at 1100 °C HTT versus fiber moduli.

The phenomenon of increased FSU with apparent interface weakening is not new to C/C. For example, Fitzer and Burger[9] found that carbonized unidirectional composites had tensile strengths that were only about one-quarter of those of the resin-matrix composites from which they were derived. They concluded that carbonization shrinkage of the matrix damaged the fibers, which led to the low composite strengths observed. However, Newling and Walker,[10] working with a very similar composite system, found that the low strengths in the carbonized state could be recovered, by as much as a factor of 3 to 5, by heat-treating the composites to 2600 °C. Later, Thomas and Walker[11] explained this strength recovery at higher HTTs as the result of formation of an interfacial layer that facilitates debonding and crack-tip blunting more effectively than in the glassy-carbon matrix. This explanation is an expression of the mechanism of toughening of brittle solids proposed by Cook and Gordon.[12]

The fracture behavior of the fibers may also contribute to the composite fracture behavior. We observed that while the fracture surfaces of the as-received E35, E75, and E105 fibers displayed smooth, planar-type fracture (shown for the E75 fiber in Fig. 6a) similar to that observed with most PAN-based fibers, the as-received E130 carbon fiber (Fig. 6b) revealed a rough, jagged fracture surface. The E130 fiber structure apparently enables each filament to behave as a composite structure, impeding crack propagation and further contributing to tough fracture beyond any contribution resulting from weakening of the interface. Such a structure is consistent with the observation that the FSU of the E130 composite is significantly higher than that for the E105 composite after 1100 °C HTT, even though the magnitudes of their ILSSs are about the same, suggesting that the fiber/matrix bond strengths in the carbonized composites should also be comparable. More graphic illustrations of the E130 fiber fracture behavior are seen in the SEMs

14

of Figs. 6c and d, which show the tensile side of a flexure specimen of the E130/1100 °C HTT at the point of incipient fracture. The specimen was mounted in a standard epoxy resin and then loaded in a special flexure stage that fits into the SEM.

Heat treatment to 2150 °C results in significant increases in strength utilization for the E75, E105, and E130 composites (Fig. 3 and Table III). The strength increases correlate roughly with increased fiber pullout, consisting mostly of clumps of filaments for the E75 composite (Fig. 7b) and well-defined pullout for the E105 and E130 (Fig. 7c) composites. The combination of increased strength and increased pullout is consistent with a mechanism of fiber/matrix interface weakening with HTT that leads to crack deflection and blunting rather than to propagation. In contrast, the E35 composite after the 2150 °C HTT still displays a relatively brittle failure (Fig. 7a), indicative of strong fiber/matrix bonding, and there is no significant change in its strength.

With HT to 2400 °C, the increase in fiber modulus, particularly for the two lower modulus fibers, and a contribution from the matrix to the composite modulus, become factors in determining the FSU [Eq. (2)]. More specifically, we see that the FSU of the E75 composite increases by 19%, with no significant change in failure strain; and for the E35 composite, FSU increases by more than 100%, in spite of a decrease in failure strain from 0.24 to 0.18%. The higher strength of the E35 composite also correlates with significant fiber pullout (Fig. 8a), indicating a weakened fiber/matrix interface relative to the lower HTTs. Another possible factor affecting FSU for the 2400 °C HTT is that the E35, E75, and E105 fibers undergo structural transformation that produces jagged fracture surfaces similar to that seen with the E130 fiber (shown for E35 in Fig. 8b). For the E130 composite, there is a significant decrease in FSU from 92 to 68%. We speculate that this strength decrease may be due to excessive weakening of the fiber/matrix interface with higher HTT, resulting in reduced matrix stress-transfer capability.

15

For the 2400 °C HTT specimens, we also observe clear definition of a well-oriented matrix sheath at the fiber/matrix interface for all the composites (illustrated in Fig. 9a for the E35 composite). The structure of the sheath, which becomes very prominent following HT to 2750 °C (Figs. 9b and c), is the result of localized graphitization of the matrix caused by matrix deformation during carbonization;[13-15] such deformation preferentially aligns the matrix, making it graphitizable in subsequent high-temperature HT.[16] This highly oriented sheath makes a significant contribution to the composite modulus, particularly at the 2750 °C HTT. It is also a factor in the significant extent of decoupling between fiber and matrix and fiber/sheath and matrix.

With HTT to 2750 °C, failure strains and FSUs decrease markedly for all the composites, probably as a result of a combination of fiber degradation and excessive fiber/ matrix debonding at such a high HTT. Fiber degradation in the form of longitudinal filament splitting (seen for the E35 fiber in Fig. 10) was evident for all of the composites. This type of filament damage was prominent only for fibers heat-treated to 2750 °C *within composites*. It is most likely a consequence of stresses induced during cooling of the fibers from this HTT. We also observed intramatrix failure within the highly aligned matrix sheath. Figure 9b shows protruded matrix "tubes" that appear to be remnants of this type of failure.

We can summarize the results of this study by stating that the strength behavior of these C/C composites over the HTT range studied is consistent with a model wherein an initially well-bonded composite, prone to matrix-dominated brittle failure, experiences a reduction in fiber/matrix bond strength with increasing HTT. Such interface weakening mitigates the tendency for brittle fracture, and works to increase fiber strength utilization. At the same time, it also results in weaker matrix-stress transfer capability, which works to reduce fiber strength utilization. At lower HTT, the gain in failure-strain capability with

16

interface weakening dominates; as a result, FSU increases. At higher HTT, and progressively weaker interface strengths and greater degrees of fiber/matrix debonding, the effect of the longer stress-transfer length dominates, and there is a general decrease in FSU.

IV. CONCLUSIONS

Fiber tensile strength utilization was studied in unidirectional C/C composites fabricated from four pitch-based fibers (E35, E75, E105, and E130) and a PAA-resin-matrix precursor. It was found that the apparent fiber failure stresses were largely determined by the initial degree of bonding between fiber and resin matrix (inferred from reported measurements of ILSS in the respective epoxy-matrix composites) and the HTT. At lower HTTs the strong fiber/matrix bond tends to be retained, which can lead to matrix-dominated brittle fracture and low FSU values. Higher HTTs lead to progressive weakening of the fiber/matrix interface as manifested by fiber pullout; the result is crack deflection and blunting, rather than propagation, and an increase in FSU. This mode of toughening appears to be related to the development of a well-oriented matrix sheath structure, which is particularly evident at higher HTTs.

Another factor affecting composite fracture behavior is the microstructure of the fibers, which can reveal extremes of fracture behavior from a brittle, planar mode to a jagged, energy-absorbing mode. All the E130 fiber composites reveal this tough fiber fracture. The other three fibers develop this same tough fracture following heat treatment to 2400 and 2750 °C. Both fiber structure and weak interface toughening mechanisms work to prevent matrix-dominated brittle fracture and, thereby, to improve FSU in the composite. With HTT to 2750 °C, FSU decreases for all the composites. This is apparently the result of processing-induced fiber degradation and reduced stress-transfer capability of the matrix. Evidence for fiber degradation in the form of longitudinal splitting is seen in SEM micrographs.

17

REFERENCES

1. J. Jortner, *Effect of Weak Interfaces on Thermostructural Behavior of C/C Composites*, Office of Naval Research Annual Report, Contract N00014-82-C-0405, pp. 19–31 (March 1985).

2. J. Jortner, "A Model for Tensile Fracture of Carbon–Carbon Composite Fiber Bundles," paper presented at the Sixth JANNAF RNTS Meeting, Huntsville, AL (December 1984); included in Ref. 1.

3. K. Leong, J. Zimmer, and R. Weitz, *Fiber Property Changes During Processing of Carbon–Carbon Composites*, Report AFWAL-TR-87-4035 (Acurex Corporation, Mountain View, CA, June 1987).

4. E. Fitzer and W. Hüttner, *J. Phys. D.: Appl. Phys.* **14**, 347 (1981).

5. H. A. Katzman, *Polyarylacetylene Resin Composites*, Report TR-0090(5935-06)-1 (The Aerospace Corporation, El Segundo, CA, April 1990).

6. R. J. Zaldivar, R. W. Kobayashi, G. S. Rellick, and J. M. Yang, *Carbon* **29**, 1145 (1991).

7. R. J. Zaldivar, G. S. Rellick, and J. M. Yang, *SAMPE J.* **27**, 29 (September/ October 1991).

8. D. Edie, R. J. Cano, and R. A. Ross, *Ext. Abstr., 20th Biennial Carbon Conf.*, p. 330 (1991).

9. E. Fitzer and A. Burger, in *Carbon Fibers: Their Composites and Applications*, p. 134 (The Plastics Inst., London, 1971).

10. D. O. Newling and E. J. Walker, in *Carbon Fibers: Their Composites and Applications*, p. 142 (The Plastics Inst., London, 1971).

11. C. R. Thomas and E. J. Walker, *High Temp.–High Press.* **10**, 79 (1978).

12. J. Cook and J. E. Gordon, *Proc. R. Soc. London* **A282**, 508 (1964).

13. R. D. Reiswig, L. S. Levinson, and J. A. O'Rourke, *Carbon* **6**, 142 (1968).

14. Y. Hishiyama, M. Inagaki, S. Kimura, and S. Yamada, *Carbon* **12**, 249 (1974).

15. R. J. Zaldivar and G. S. Rellick, *Carbon* **29**, 1155 (1991).

16. G. S. Rellick, D. J. Chang, and R. J. Zaldivar, *J. Mater. Res.* accepted for publication.

Table I. Manufacturer's Test Results on Dupont E-series fibers

Fiber	Modulus (GPa)	Strength (GPa)		Fiber Diameter (μm)
		Single Filament[a]	Impregnated Strand[b]	
E130	894	3.8	2.7	9.2
E105	724	3.1	2.6	9.6
E75	516	3.1	2.4	9.6
E35	241	2.9	2.5	10.0

[a]1-in. gauge length. No surface treatment or sizing.
[b]6-in. gauge length. ASTM D4018.

Table II. Changes in (002) d-spacing (nm) with heat-treatment temperature (HTT) for E-series fibers.

Fiber	Heat-Treatment Temperature (°C)				
	As-received	1100	2150	2400	2750
E130	0.338	0.338	0.338	0.338	0.337
E105	0.343	0.343	0.339	0.338	0.337
E75	0.343	0.343	0.339	0.338	0.337
E35	0.347	0.347	0.339	0.338	0.337

TABLE III. Apparent fiber failure strains and fiber strength utilization (FSU) values for different composites, by HTT.[a]

Fiber	Failure strain (%) and FSU (%) by HTT									
	Cured Resin		1100 °C		2150 °C		2400 °C		2750 °C	
E35	0.90	100	0.20	24	0.24	28	0.18	60	0.09	31
E75	0.40	100	0.09	24	0.21	62	0.22	74	0.07	28
E105	0.30	100	0.11	35	0.21	72	0.22	74	0.09	34
E130	0.25	100	0.22	79	0.24	92	0.21	68	0.14	42

[a] All values of FSU are calculated relative to the heat-treated fiber strengths, and all, except for the 2750 °C HTT, are calculated assuming all the composite load is carried by the fibers. For 2750 °C HTT, we estimate that the fibers carry 73% of the load.
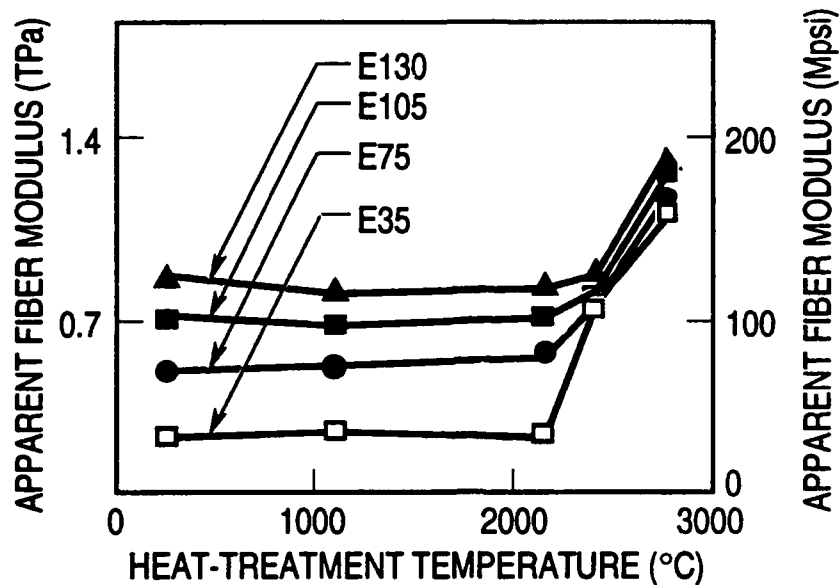
Figure 1. Apparent fiber moduli, calculated from rule-of-mixtures model, assuming $E_c \cong E_f V_f$, of PAA-resin-matrix composites and C/C composites heat treated to various temperatures. Standard deviations (SDs)) were about 5 to 12 Mpsi and increased with HTT. Coefficients of variation (CV) varied from 4 to 15% and were generally larger for the lower modulus fibers.
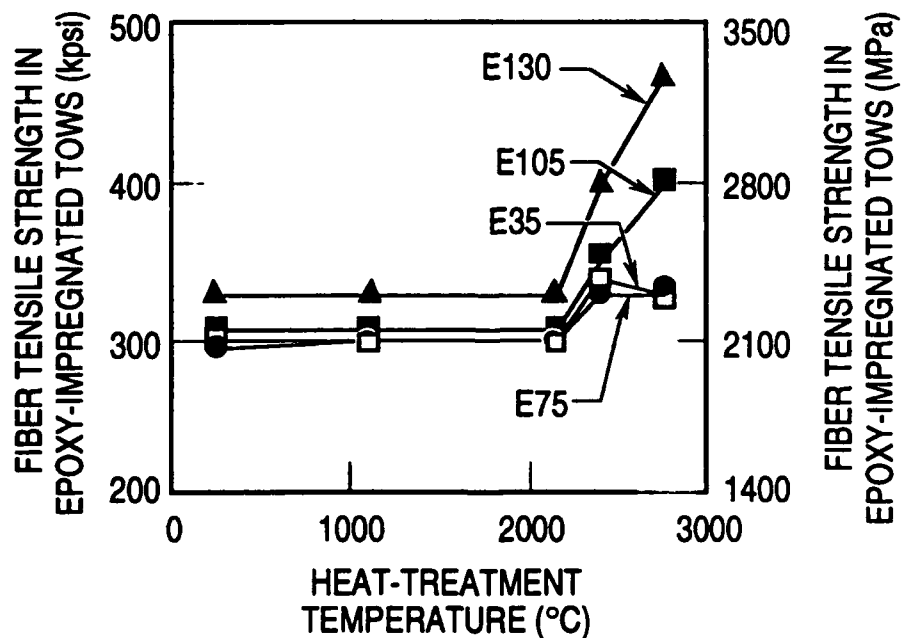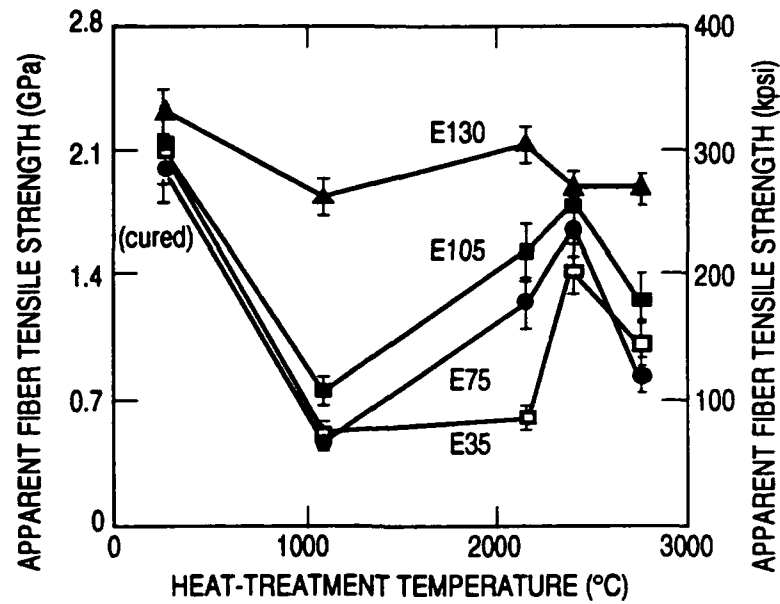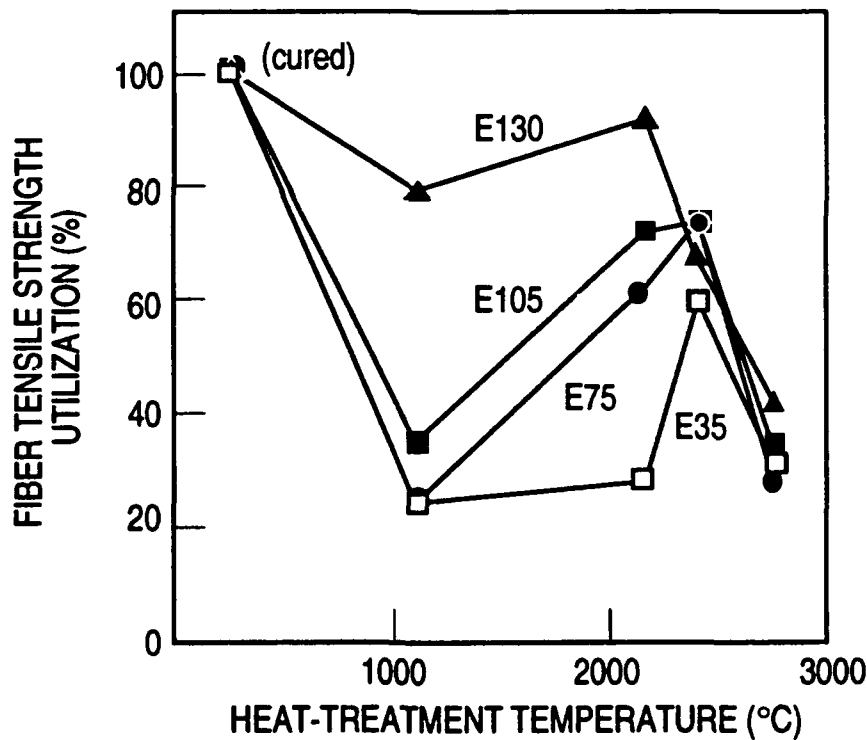

Figure 2. Tensile strength of fibers in epoxy-impregnated bundles as a function of fiber heat-treatment temperatures. SD ≈ 7 to 9 kpsi; CV ≈ 2 to 4%.
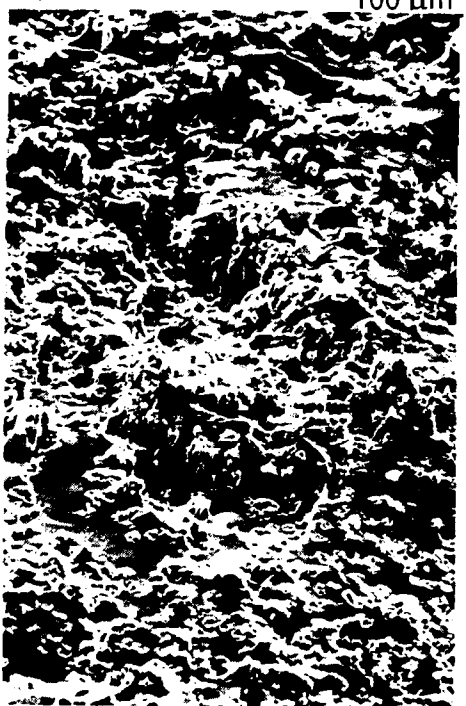
24

Figure 3. (a) Apparent fiber strengths and (b) fiber strength utilizations (FSU) of E35, E75, E105, and E130 fiber composites heat treated to various temperatures. FSU is based on strengths of heat-treated fibers. SD ≈ 3 to 9 kpsi; CV ≈ 3 to 10%, increasing generally with HTT.

25
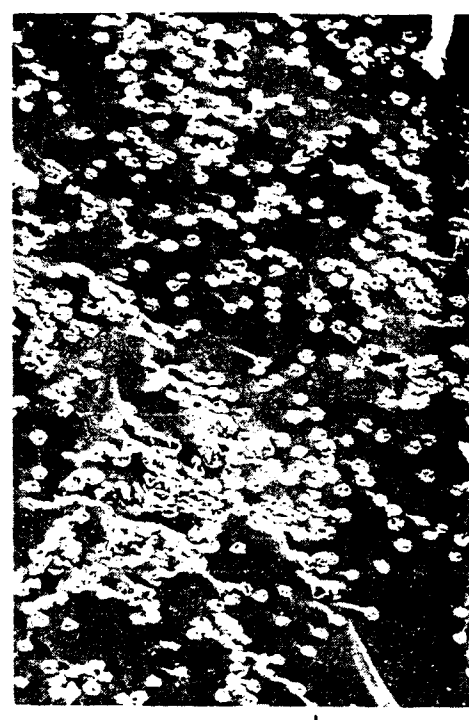
(a)　100 μm

(b)　100 μm

(c)　100 μm

(d)　1υ0 μm

Figure 4.　Fracture surfaces of C/C composites heat treated to 1100°C:　(a) E35, (b) E75, (c) E105, and (d) E130.
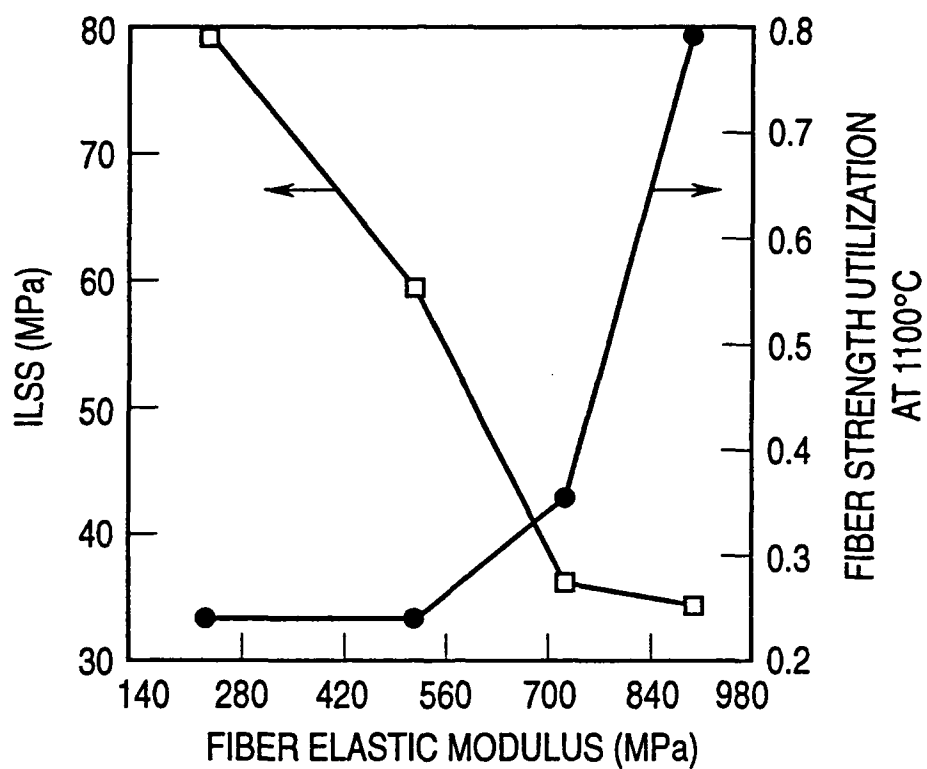
26

Figure 5. Plots of interlaminar shear strength (ILSS) of cured-resin composites (from Ref. 8) and C/C fiber strength utilizations for 1100°C HTT for various fibers vs fiber moduli.
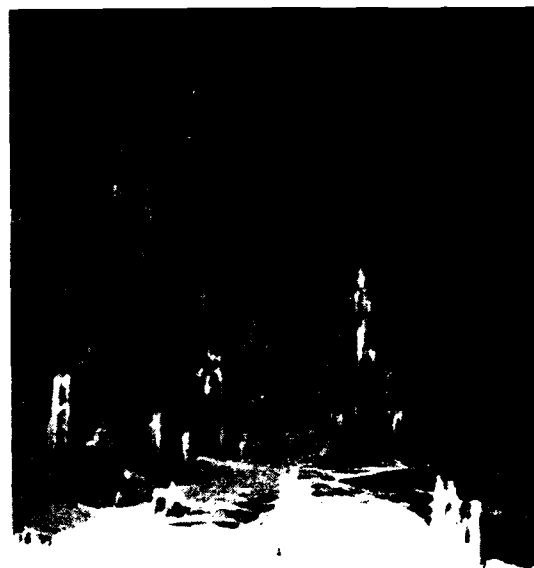
Figure 6. Fracture surfaces of fibers in resin-matrix composites: (a) E75 as-received, (b) E130 as-received (c) and (d) real-time fraacture of 1100°C HTT E130 composite observed in SEM flexure stage.
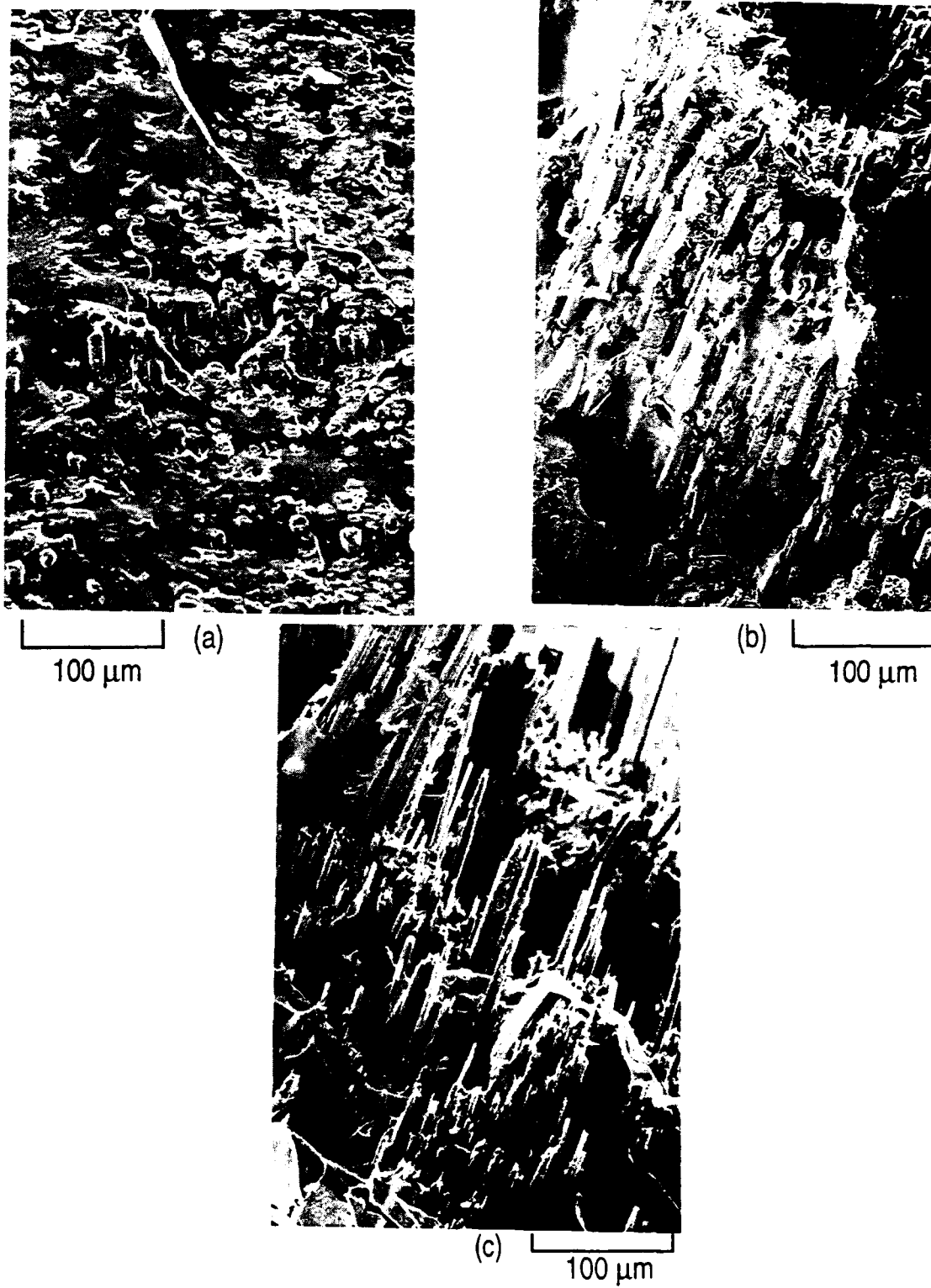
28

Figure 7. Fracture surfaces of C/C composites heat treated to 2150°C: (a) E35, (b) E75, and (c) E130.

(a)   100 μm   (b)   10 μm

Figure 8. Fracture surface of E35/PAA-derived C/C composite heat treated to 2400°C: (a) low magnification and (b) hign magnification, showing filament structure.
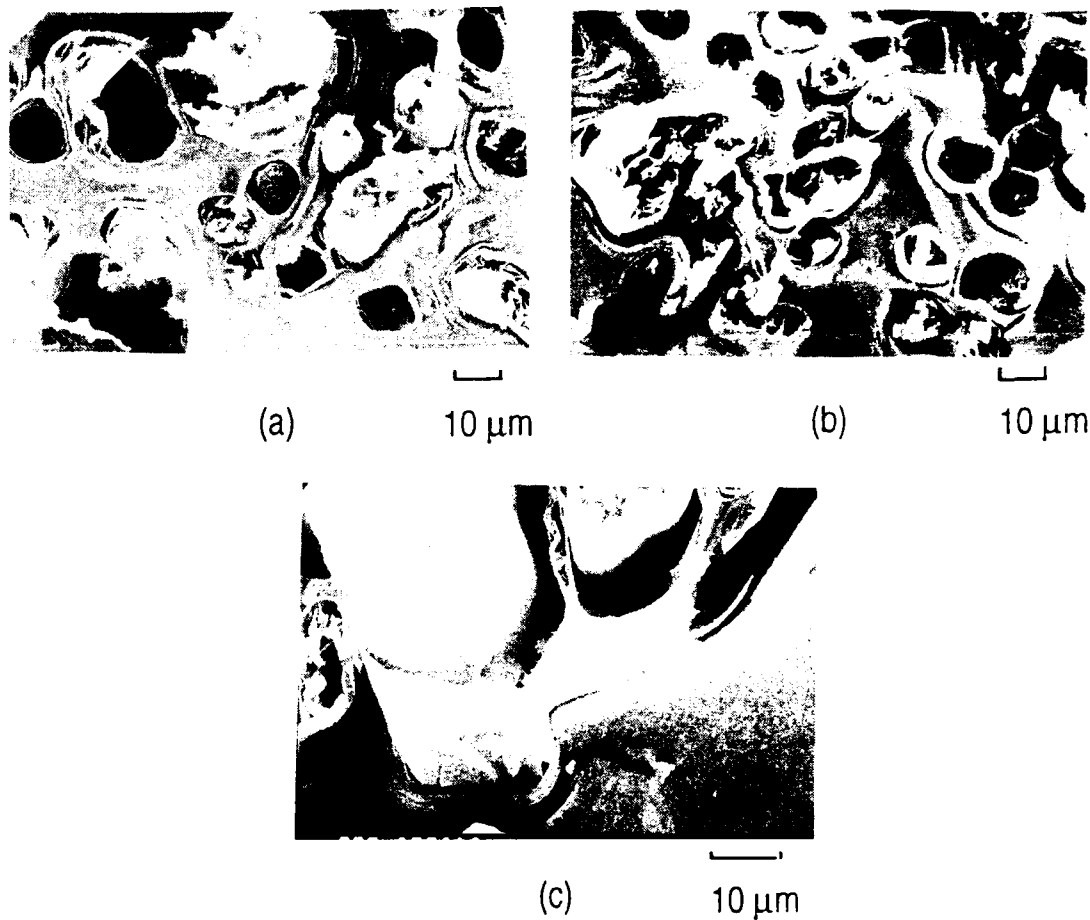
(a)　10 μm　(b)　10 μm

(c)　10 μm

Figure 9. Fracture surface of (a) E35 composite heat treated to 2400°C, (b) E105 composite heat treated to 2750°C, and (c) E35 composite heat treated to 2750°C.
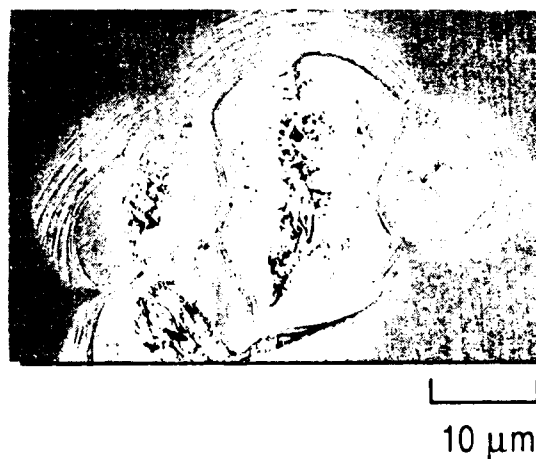

10 μm

Figure 10. SEM of polished, ion-etched cross section of E35 C/C composite heat treated to 275°C, showing longitudinal filament splitting

31

TECHNOLOGY OPERATIONS

The Aerospace Corporation functions as an "architect-engineer" for national security programs, specializing in advanced military space systems. The Corporation's Technology Operations supports the effective and timely development and operation of national security systems through scientific research and the application of advanced technology. Vital to the success of the Corporation is the technical staff's wide-ranging expertise and its ability to stay abreast of new technological developments and program support issues associated with rapidly evolving space systems. Contributing capabilities are provided by these individual Technology Centers:

Electronics Technology Center: Microelectronics, solid-state device physics, VLSI reliability, compound semiconductors, radiation hardening, data storage technologies, infrared detector devices and testing; electro-optics, quantum electronics, solid-state lasers, optical propagation and communications; cw and pulsed chemical laser development, optical resonators, beam control, atmospheric propagation, and laser effects and countermeasures; atomic frequency standards, applied laser spectroscopy, laser chemistry, laser optoelectronics, phase conjugation and coherent imaging, solar cell physics, battery electrochemistry, battery testing and evaluation.

Mechanics and Materials Technology Center: Evaluation and characterization of new materials: metals, alloys, ceramics, polymers and their composites, and new forms of carbon; development and analysis of thin films and deposition techniques; nondestructive evaluation, component failure analysis and reliability; fracture mechanics and stress corrosion; development and evaluation of hardened components; analysis and evaluation of materials at cryogenic and elevated temperatures; launch vehicle and reentry fluid mechanics, heat transfer and flight dynamics; chemical and electric propulsion; spacecraft structural mechanics, spacecraft survivability and vulnerability assessment; contamination, thermal and structural control; high temperature thermomechanics, gas kinetics and radiation; lubrication and surface phenomena.

Space and Environment Technology Center: Magnetospheric, auroral and cosmic ray physics, wave-particle interactions, magnetospheric plasma waves; atmospheric and ionospheric physics, density and composition of the upper atmosphere, remote sensing using atmospheric radiation; solar physics, infrared astronomy, infrared signature analysis; effects of solar activity, magnetic storms and nuclear explosions on the earth's atmosphere, ionosphere and magnetosphere; effects of electromagnetic and particulate radiations on space systems; space instrumentation; propellant chemistry, chemical dynamics, environmental chemistry, trace detection; atmospheric chemical reactions, atmospheric optics, light scattering, state-specific chemical reactions and radiative signatures of missile plumes, and sensor out-of-field-of-view rejection.